PERFORMANCE LIMITATIONS FOR THE PHASE SCREEN IN THE SETTINGS OF TRANSIONOSPHERIC SAR

*Mikhail Gilman**

North Carolina State University
Department of Mathematics
NCSU, Box 8205,
Raleigh, NC 27695, USA

Semyon Tsynkov

North Carolina State University
Department of Mathematics
NCSU, Box 8205,
Raleigh, NC 27695, USA

ABSTRACT

Low-frequency transionospheric radar is affected by large- and small-scale inhomogeneities of the ionospheric electron number density causing phase perturbations of the radar pulses. These perturbations may lead to distortions in the synthetic aperture radar (SAR) images. Phase corrections may be implemented by means of a phase screen, which is an approximation of the actual "thick" ionosphere by an infinitesimally thin layer of plasma. We evaluate the accuracy that can be achieved using such a representation. We will consider a large-scale setup due to the atmospheric gravity wave and a small-scale scenario represented by the turbulence.

Index Terms— SAR imaging, autofocus, ionosphere

1. INTRODUCTION

Transionospheric synthetic aperture radar (SAR) imaging is prone to phase perturbations due to the dispersion of electromagnetic waves in the ionospheric plasma. The radar pulses, as they propagate through the Earth's ionosphere, experience the phase advance and group delay, both proportional to the local electron number density. The total phase advance and group delay are thus proportional to the integral of the electron number density over the ray path. In the context of SAR signal processing these phase perturbations, if severe enough, may degrade the quality of the resulting SAR images [1, 2, 3, 4, 5].

A number of approaches to mitigate the above effects have been suggested. Typically, a phase correction term is introduced into the matched filter such that both the phase advance and group delay are compensated. If the ionosphere is inhomogeneous, this correction should be made individually for every antenna and image location. A common approach involves a phase screen at a certain elevation, typically at about $350\,km$, which is roughly the altitude of the maximum of the ionospheric electron number density. The screen is a horizontal plane, and the screen density is a function of two horizontal coordinates. For a given antenna and image location, the phase correction is the value of the screen density function taken at the intersection between the ray path and the screen.

Since the actual ionosphere is three-dimensional, its representation by a two-dimensional function may be deficient, in the sense that phase distortions realized by the actual three-dimensional electron number density function cannot be matched by those realized by a phase screen for all ray paths at once. The level of the corresponding residual distortions can serve as a metric for the quality of approximation of the Earth's ionosphere by a phase screen.

The ionospheric plasma can support a large variety of disturbances. The most important characteristics of ionospheric perturbations for this study are the magnitude and spatial scale. As far as the spatial scales are concerned, we will analyze two cases. The first case is where the characteristic scale of the inhomogeneity is significantly larger than the length of the synthetic aperture; a typical example is a traveling ionospheric disturbance (TID), which is an ionospheric manifestation of the atmospheric gravity wave. We evaluate the effect using observations of TIDs reported in [6]. The opposite case is that of a turbulence with the scales much smaller than the length of the synthetic aperture, and we use the ionospheric parameters adopted in [1].

2. PHASE PERTURBATION DUE TO DISPERSIVE PROPAGATION IN THE IONOSPHERE

Propagation of electromagnetic waves in plasma is dispersive: the phase and group velocities depend on the signal frequency ω:

$$v_{\text{ph}} \approx c\Big(1+\frac{\omega_{\text{pe}}^2}{2\omega^2}\Big), \quad v_{\text{gr}} \approx c\Big(1-\frac{\omega_{\text{pe}}^2}{2\omega^2}\Big), \tag{1}$$

where c is the speed of light and

$$\omega_{\text{pe}}^2 = \frac{4\pi e^2}{m_{\text{e}}} N_{\text{e}} \ll \omega^2 \tag{2}$$

*This work was supported by the US Air Force Office of Scientific Research (AFOSR) under grants FA9550-21-1-0086 & FA9550-23-1-0101.

is the plasma frequency. In formulae (1) and (2), $m_{\rm e}$ and $-e$ are the electron mass and charge, respectively, and $N_{\rm e}$ is the electron number density.

The Earth's ionosphere is inhomogeneous, which means that $N_{\rm e}$ in (2) is a function of the coordinates. We will consider the slant plane such that the antenna and target coordinates are represented as $\boldsymbol{x} = (x, R)$ and $\boldsymbol{z} = (z, 0)$, respectively, where R is the standoff distance. In the following expressions for the one-way phase and group travel times:

$$\begin{aligned} T_{\rm ph}(\boldsymbol{x}, \boldsymbol{z}) &\approx \frac{|\boldsymbol{x} - \boldsymbol{z}| - \varphi(\boldsymbol{x}, \boldsymbol{z})/2}{c}, \\ T_{\rm gr}(\boldsymbol{x}, \boldsymbol{z}) &\approx \frac{|\boldsymbol{x} - \boldsymbol{z}| + \varphi(\boldsymbol{x}, \boldsymbol{z})/2}{c}, \end{aligned} \tag{3}$$

the perturbation of the eikonal φ is given by

$$\varphi(\boldsymbol{x}, \boldsymbol{z}) \approx \frac{4\pi e^2}{m_{\rm e}\omega_0^2} |\boldsymbol{x} - \boldsymbol{z}| \int_0^1 N_{\rm e}(\zeta)\, {\rm d}\zeta \tag{4}$$

with

$$N_{\rm e}(\zeta) \equiv N_{\rm e}(\zeta; \boldsymbol{x}, \boldsymbol{z}) = N_{\rm e}\big(\zeta \boldsymbol{x} + (1 - \zeta)\boldsymbol{z}\big), \tag{5}$$

see (1) and (2).

The SAR image $I(\boldsymbol{y}) \equiv I(y)$, where $\boldsymbol{y} = (y, 0)$, is an approximate reconstruction of the reflectivity function $\nu(z)$ using a matched filter. The standard matched filter compensates the propagation phase, with the expression for the distance given by

$$|\boldsymbol{x} - \boldsymbol{z}| \approx R + \frac{(x - z)^2}{2R}.$$

The reconstruction term $\varphi^{\rm rec}$ used in addition to the propagation phase is designed to mitigate the distortions and realized by the screen density function $\varphi_{\rm S}$:

$$\varphi^{\rm rec}(\boldsymbol{x}, \boldsymbol{y}) = Q\varphi_{\rm S}\big(s(\boldsymbol{x}, \boldsymbol{y})\big) \equiv Q\varphi_{\rm S}\big(\xi x + (1 - \xi)y\big). \tag{6}$$

In (6), ξ is the screen elevation relative to the orbit height [cf. (5)], and $Q = Q(\boldsymbol{x} - \boldsymbol{y}) = \sqrt{1 + b^2}$, where

$$b = (x - z)/R.$$

Thus, Q is a geometric factor due to the squint that is independent of the ionosphere, and $s(\boldsymbol{x}, \boldsymbol{y})$ is the horizontal coordinate of the intersection between the screen and the ray connecting $\boldsymbol{x}$ and $\boldsymbol{y}$. Note that $N_{\rm e}(s, h)$ in (5) is a bivariate function whereas $\varphi_{\rm S}(s)$ in (6) is a univariate function. We make a natural choice for the phase screen to exactly compensate the broadside rays (i.e., those where $x = y$). This means that [cf. (4)]

$$\varphi_{\rm S}(s) = \frac{4\pi e^2}{m_{\rm e}\omega_0^2} \frac{1}{\cos\theta} \int_0^{R\cos\theta} N_{\rm e}(s, h)\, {\rm d}h, \tag{7}$$

where θ is the angle between the normal to the slant plane and the vertical direction.

The image $I(y)$ is given by convolution of the reflectivity $\nu(z)$ with the imaging kernel $W(y, z)$ [7, 8]:

$$I(y) = \int \nu(z) W(y, z)\, {\rm d}z,$$

where

$$\begin{aligned} W(y, z) = \frac{1}{N} \sum_{x_j \in \mathbf{D}_{yz}} \exp\Big[2ik \frac{y - z}{R}\Big(x_j - \frac{y + z}{2}\Big)\Big] \\ \cdot \exp\big[-ik\big(\varphi(x_j, z) - \varphi^{\rm rec}(s_j)\big)\big]. \end{aligned} \tag{8}$$

In equation (8), $k = \omega_0/c$ is the carrier wavenumber, and $s_j \equiv s(x_j, y) = \xi x_j + (1 - \xi)y$, cf. (6). The domain of antenna locations $\mathbf{D}_{yz}$ in (8) is defined as $\mathbf{D}_{yz} = \{x |\ (|x - y| \le L_{\rm SA}/2)$ and $(|x - z| \le L_{\rm SA}/2)\}$, where $L_{\rm SA}$ is the length of the synthetic aperture. In the absence of phase perturbations $T_{\rm ph}(\boldsymbol{x}, \boldsymbol{z}) = T_{\rm gr}(\boldsymbol{x}, \boldsymbol{z}) = |\boldsymbol{x} - \boldsymbol{z}|/c$, and the first line in formula (8) results in the standard imaging kernel

$$W_0(y, z) \approx {\rm sinc}\Big(kL_{\rm SA} \frac{y - z}{R}\Big). \tag{9}$$

When the perturbations due to the ionosphere are present and compensated by a phase screen as in (6)–(7), the second line in (8) represents residual distortions, the level of which depends on many factors. In Sections 3 and 4 below, we analyze the geophysical scenarios corresponding to large and small spatial scales, respectively.

3. LARGE-SCALE PERTURBATIONS

As an example of large-scale perturbation of the ionosphere, we will consider a traveling ionospheric disturbance (TID), for which the horizontal scale may exceed $10^3\, km$ [9]. This scale is much larger than the length of the synthetic aperture $L_{\rm SA}$, so the following expansion for the electron number density is possible:

$$N_{\rm e}(s, h) \approx N_0(h) + N_1(h)s + N_2(h)s^2. \tag{10}$$

We will evaluate the ionosphere-related terms in (8) using (3), (4), (6), and (10). Introducing $H = R\cos\theta$,

$$\begin{aligned} \mathcal{U}_a &= \int N_1(h)(h - \xi H)\, {\rm d}h, \\ \mathcal{U}_b &= \int N_2(h)(h - \xi H)\, {\rm d}h, \\ \mathcal{U}_c &= \int N_2(h)\big(h^2 - (\xi H)^2\big)\, {\rm d}h, \end{aligned}$$

we express the leading order terms of the residual phase in (8) as follows:

$$\begin{aligned} k\big(\varphi(x_j, z) - \varphi^{\rm rec}(x_j, z)\big) = k \frac{4\pi e^2}{m_{\rm e}\omega_0^2} \frac{\sqrt{1 + b^2}}{\cos\theta} \\ \cdot \Big[\frac{x_j - z}{H\cos\theta}(\mathcal{U}_a + 2z\mathcal{U}_b) + \Big(\frac{x_j - z}{H\cos\theta}\Big)^2 \mathcal{U}_c\Big]. \end{aligned} \tag{11}$$

When substituted into the sum in (8), the terms proportional to x_j in (11) result in a shift of the image in the cross-range (azimuthal) direction: $y = z + z_{\text{shift}}$, where

$$z_{\text{shift}} = \frac{\sqrt{1+b^2}}{2\cos^2\theta}\,\frac{4\pi e^2}{m_e\omega_0^2}\Big[\mathcal{U}_a + 2z\Big(\mathcal{U}_b - \frac{1}{H\cos\theta}\mathcal{U}_c\Big)\Big]. \quad (12)$$

Depending on the sign of $\mathcal{U}_b$, the second term in the parentheses in (12) describes stretching or compression of the image in the cross-range direction.

Another source of distortions is the term containing x_j^2 that results in the azimuthal defocusing. Taken at $|x_j - z| = L_{\text{SA}}/2$, this term yields the quadratic phase error (QPE) that is commonly used as a measure of this type of distortion.

In order to estimate the level of the resulting distortions, we will use the parameters of TID as reported in [6] where the electron number density dropped by about 30% from the initial value of $N_e \approx 7\cdot 10^{11}\,m^{-3}$. We also take $200km$ as a total thickness of the plasma layer [10], $\xi H = 350km$, and the vertical TEC of about 10 TECU $\equiv 10\cdot 10^{16}\,m^{-2}$ as in [6]. The radar parameters are the same as in [1, Table 1.1], in particular, $\omega_0 = 300MHz$, $L_{\text{SA}} = 5\cdot 10^4 m$, $R = 10^6 m$, and $\cos\theta = 1/2$. The resulting distortions are characterized by the stretching/compression coefficient: $|\partial z_{\text{shift}}/\partial z| < 10^{-4}$, whereas for the defocusing measure, we obtain QPE < 0.2. Altogether, the level of residual distortions of the image is low. This means that the phase screen approach is quite adequate for compensating the phase errors due to TIDs.

4. SMALL-SCALE PERTURBATIONS

The turbulence is usually considered in a stochastic framework. This means that the ionospheric density function N_e is sampled from a certain distribution. The most important characteristics of this distribution are the level of fluctuations $\langle\mu^2\rangle = \big\langle(N_e - \langle N_e\rangle)^2\big\rangle$ and the correlation radius $r_0 \sim 1$–$10\,km$. In turn, all expressions involving N_e, including the eikonal perturbations (4) and (7), become random as well and will be characterized via their lower moments. In particular, the variance of the one-way eikonal in (4) will be represented by a dimensionless parameter $\mathcal{D}^2$:

$$\mathcal{D}^2 = k^2\langle\varphi^2\rangle/2. \quad (13)$$

The value of $\mathcal{D}^2$ can be expressed via $\langle\mu^2\rangle$, r_0, and the propagation distance, see [1, Table 1.2 and Section 4].

In order to describe statistical properties of the imaging kernel given by (8), we will employ the clustering approach [11] where the rays passing through the turbulent plasma layer are grouped into clusters such that the horizontal distance between them does not exceed r_0, see Figure 1. It can be shown that the correlation radius of the eikonal is also r_0, see [1, Chapter 4]. Hence, as a rough approximation, we consider the phase perturbations for any two rays in one cluster identical, whereas in different clusters, independent.

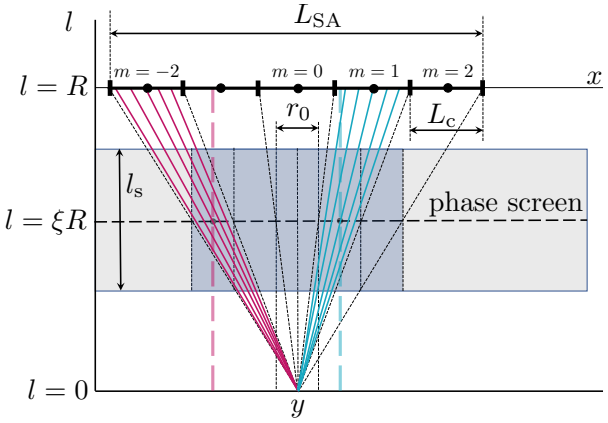

Fig. 1. Clustering approach for the analysis of transionospheric SAR with turbulence. The rays corresponding to one and the same cluster are indicated by the lines having the same color. The solid and dashed lines correspond to φ and φ^{rec} in (8), respectively. Angles are not to scale.

In what follows, we will use m as the cluster index. Introduce

$$\phi_m(y,z) = \varphi(x_m,z) - \varphi^{\text{rec}}(s_m), \quad (14)$$

cf. (8), where

$$x_m = y + mr_0/\xi, \quad s_m = y + mr_0.$$

We assume that with $|b| \ll 1$ and the resolution size being much smaller than the ionospheric scale, the expression for the residual phase in (14) can be simplified: $\phi_m(y,z) \approx \phi_m(y,y) \equiv \phi_m(y)$. Using the clustering assumptions above, we reorganize the sum in (8) into a sum over the clusters:

$$W(y,z) = \sum_m U_m(y,z)\exp(-\mathrm{i}k\phi_m). \quad (15)$$

The terms U_m in (15) are deterministic and can be obtained by performing summation within each cluster:

$$U_m \approx \frac{r_0}{\xi L_{\text{SA}}}\exp(2\mathrm{i}m\eta)\,\operatorname{sinc}\eta,$$

where [cf. (9)]

$$\eta = \frac{kr_0(y-z)}{\xi R}.$$

Assuming that the statistics of the eikonals is Gaussian, we derive the following expressions for the lower moments of $W(y,z)$ in (15):

$$\langle W(y,z)\rangle = \frac{r_0}{\xi L_{\text{SA}}}\operatorname{sinc}\eta\sum_m \exp(2\mathrm{i}m\eta)\exp(-\mathcal{D}_m^2) \quad (16)$$

and

$$\operatorname{std}\big[W(y,z)\big] = \big\langle|W(y,z) - \langle W(y,z)\rangle|^2\big\rangle^{1/2}$$
$$= \frac{r_0}{\xi L_{\text{SA}}}\operatorname{sinc}\eta\Big[\sum_m\big[1-\exp(-2\mathcal{D}_m^2)\big]\Big]^{1/2}, \quad (17)$$

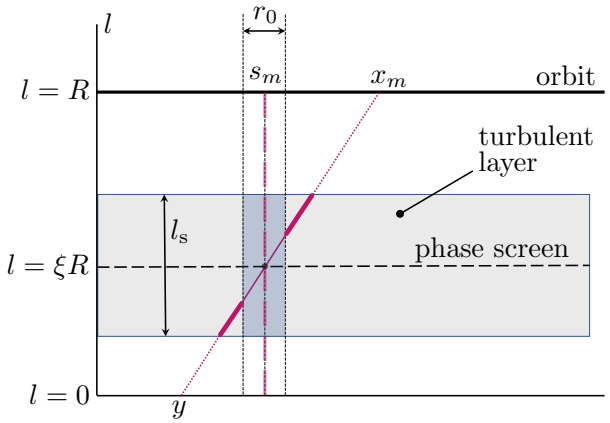

Fig. 2. Geometry of the rays corresponding to φ (the oblique line) and φ^{rec} (the dashed vertical line). The thin solid segment of the oblique line indicates the part of the ray where the values of $N_e(\cdot, h)$ contributing to φ and φ^{rec} are considered equal, whereas for the thick segments, uncorrelated.

see [1, Chapter 4], where [cf. (13)]

$$\mathcal{D}_m^2 = \frac{k^2\langle\phi_m^2\rangle}{2} = \frac{k^2\langle\left(\varphi(x_m, y) - \varphi^{\text{rec}}(s_m)\right)^2\rangle}{2}. \quad (18)$$

We will obtain a rough estimate of $\mathcal{D}_m^2$ using the geometric considerations illustrated by Figure 2. The perturbation φ and correction φ^{rec} eikonals correspond to the oblique and vertical (dashed) colored lines, respectively. For the oblique ray, the thin/thick solid segments indicate the parts where the perturbations are fully correlated/uncorrelated with those on the vertical line. We will estimate the correlation coefficient between φ and φ^{rec} from the proportions of the lengths of these segments as follows. Let $l_s = h_s/\cos\theta$ be the distance that the rays travel through the turbulent layer, where $h_s \sim 50km \gg r_0$ is the thickness of this layer [10], and define $b_s = r_0/l_s$ as the critical squint angle such that the rays representing φ and φ^{rec} are never separated by more than r_0 while within the turbulent layer. Then the cluster size at the orbit is Rb_s, $m = [b/b_s]$ where $[\ldots]$ is the integer part, and from the similarity of triangles, we have

$$\rho_m = \frac{\langle\varphi(x_m, y)\varphi^{\text{rec}}(s_m)\rangle}{\langle\varphi^2\rangle} \approx \begin{cases} 1 & \text{if } m = 0, \\ \dfrac{1}{|m|} & \text{otherwise.} \end{cases} \quad (19)$$

Further, from (18) and (19), we obtain

$$\mathcal{D}_m^2 = 2\mathcal{D}^2(1 - \rho_m). \quad (20)$$

Figure 3 plots the curves obtained by substituting (20) into (16) and (17) and performing summation. From the plots of $\langle W\rangle$ we can observe the decrease of the average peak height as compared to the unperturbed case of $\mathcal{D}^2 = 0$ given by (9) where $W(0) \equiv W(y, y) = 1$. In turn, comparing the plots of $\langle W\rangle$ with those of $\text{std}[W]$, we see that outside of the central peak the latter may dominate. When this is the case, the sidelobes should be calculated using formula (17) rather than (16).

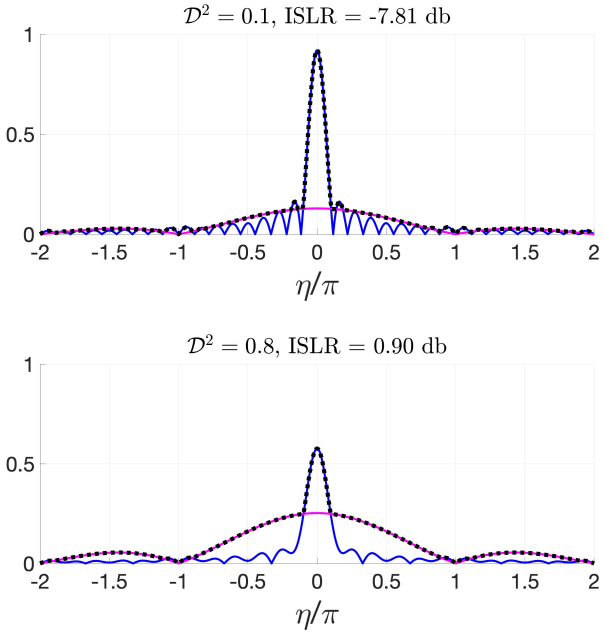

Fig. 3. The imaging kernels for the transionospheric SAR in the case of ionospheric turbulence for $m = -4, -3, \ldots, 3, 4$ (9 clusters in total). The blue and purple curves are the mean and std of W calculated according to (16) and (17), respectively. The ISLR values are computed from the maximum of these functions (black dotted curves).

Qualitatively, Figure 3 shows that in the case of turbulence, the compensation of distortions by a phase screen is not as efficient as for large-scale perturbations considered in Section 3, and when the level of phase fluctuations is large, the image distortions may be significant. One option to provide numerical characterization to the deterioration of the resulting SAR images is to calculate integrated sidelobe ratio (ISLR, see [12]) of the effective imaging kernel (shown in black dotted lines in Figure 3). While for the unperturbed kernel [i.e., $\mathcal{D}^2 = 0$, see (9)] we have ISLR $\approx -9.68db$, the cases of $\mathcal{D}^2 = 0.1$ and $\mathcal{D}^2 = 0.8$ illustrated in Figure 3 yield ISLR $\approx -7.81db$ and ISLR $= 0.90db$, respectively.

5. SUMMARY

In this work we have studied the effectiveness of a phase screen in compensating the phase perturbations due to the dispersion in the Earth's ionosphere. We have found that in the case of ionospheric turbulence, even if phase screen compensate exactly the perturbations for the broadside propagation, the image distortions may be significant. In such cases, more complicated models of transionospheric propagation may be warranted.

6. REFERENCES

[1] Mikhail Gilman, Erick Smith, and Semyon Tsynkov, *Transionospheric synthetic aperture imaging*, Applied and Numerical Harmonic Analysis. Birkhäuser/Springer, Cham, Switzerland, 2017.

[2] F. J. Meyer, "Performance requirements for ionospheric correction of low-frequency SAR data," *IEEE Transactions on Geoscience and Remote Sensing*, vol. 49, no. 10, pp. 3694–3702, October 2011.

[3] Paul A. Rosen, Scott Hensley, and Curtis Chen, "Measurement and mitigation of the ionosphere in L-band interferometric SAR data," in *Proceedings of the IEEE International Radar Conference*, Arlington, VA, 2010, pp. 1459–1463.

[4] Jingyi Chen and Howad A. Zebker, "Ionospheric artifacts in simulataneous L-band InSAR and GPS observations," *IEEE Transactions on Geoscience and Remote Sensing*, vol. 50, no. 4, pp. 1227–1239, April 2012.

[5] Jun Su Kim, Andreas Danklmayer, and Konstantinos Papathanassiou, "Correction of ionospheric distortions in low frequency interferometric SAR data," in *Proceedings of the 2011 IEEE International Geoscience and Remote Sensing Symposium (IGARSS'11)*. IEEE, 2011, pp. 1505–1508.

[6] Gottfried Kirchengast, Klemens Hocke, and Kristian Schlegel, "Gravity waves determined by modeling of traveling ionospheric disturbances in incoherent-scatter radar measurements," *Radio science*, vol. 30, no. 5, pp. 1551–1567, 1995.

[7] Mikhail Gilman and Semyon V. Tsynkov, "Transionospheric Autofocus for Synthetic Aperture Radar," *SIAM J. Imaging Sci.*, vol. 16, no. 4, pp. 2144–2174, 2023.

[8] Mikhail Gilman and Semyon Tsynkov, "Modeling the Earth's ionosphere by a phase screen for the analysis of transionospheric SAR imaging," *IEEE Trans. Geosci. Remote Sens.*, vol. 62, pp. Article Sequence Number 2000216 (16 pp), 2024.

[9] K Hocke and K Schlegel, "A review of atmospheric gravity waves and travelling ionospheric disturbances: 1982–1995," *Annales Geophysicae*, vol. 14, no. 9, pp. 917–940, 1996.

[10] Thomas D Damon and Franklin R Hartranft, "Ionospheric electron density profile model," Tech. Rep., Weather Wing (4th) ENT AFB CO Detachment 1, 1970.

[11] S. V. Tsynkov, "On SAR imaging through the Earth's ionosphere," *SIAM J. Imaging Sci.*, vol. 2, no. 1, pp. 140–182, 2009.

[12] Ian G. Cumming and Frank H. Wong, *Digital Processing of Synthetic Aperture Radar Data. Algorithms and Implementation*, Artech House, Boston, 2005.